

Statistical Image Reconstruction with Sample-Based Beam-Hardening compensation for X-ray CT

C. Martinez, J. A. Fessler, M. Desco, and M. Abella

Abstract— CT images are often affected by beam-hardening artifacts due to the polychromatic nature of the X-ray spectra. These artifacts appear in the image as cupping in homogeneous areas and streaks between dense parts in heterogeneous samples.

This paper proposes a new statistical reconstruction method for X-ray CT based on Poisson statistics, taking into account the non-linearities caused by beam hardening. To avoid needing knowledge of the X-ray spectrum, the method obtains the 2D beam-hardening function using information provided by the acquired data itself.

Evaluation using simulations showed beam hardening artifact reductions similar to those achieved with conventional post-processing techniques while avoiding noise and artifacts in low-dose studies.

Index Terms—Beam-hardening, CT, artifacts, penalized-likelihood, streaks, polychromatic.

INTRODUCTION

The beam hardening effect in computed tomography derives from the polychromatic nature of the radiation produced by X-ray tubes. Due to the energy dependence of mass attenuation coefficients, low energy photons are preferably absorbed, causing a shift of the mean energy of the X-ray beam to higher values. This effect leads to two main artifacts in uncorrected reconstructed images: cupping in homogeneous regions and streaks between dense areas in heterogeneous regions [1].

Several strategies can be found in the literature to compensate for this effect. Physical filters are generally used to pre-harden the beam before reaching the sample, but this is not enough to remove the artifacts. Another method implemented in most commercial scanners is the water-

linearization, based on a prior calibration with a water-equivalent phantom. This method models the object as homogeneous and corrects only cupping artifact [2]. To correct also streaks, Nalcioglu et al. [3] proposed a method that requires knowledge of the spectrum, the linear attenuation coefficients and the thickness of soft tissue and bone traversed estimated by means of a preliminary reconstruction. Joseph et al. [4] proposed a similar idea modeling the corrected data with a second-order polynomial dependent on the bone traversed thickness. However, the optimum parameters for this model could be exactly obtained only with a complete characterization of the spectrum. This need of knowledge of the spectra was avoided in [5, 6], also based on a linear combination of basis images to correct streaks. The coefficients of this linear combination are obtained iteratively maximizing the flatness of the soft tissue areas, which could reduce the soft-tissue contrast. Cupping correction is achieved using the water-linearization method, which needs a calibration step. We recently proposed two new methods extending the water-linearization to a 2D linearization [7, 8]. However, they require a good bone and soft tissue segmentation which may hinder their use in low-dose studies.

To deal with low-dose studies, Elbrakri et al. presented a statistical method that requires knowledge of the spectrum [9, 10]. This is avoided in [11, 12] with a simplified statistical algorithm that parametrizes the beam-hardening function following the model proposed by Joseph and Spital [4].

This paper presents a variation of [12] that replaces the approximation functions with the real measured line integrals of bone and soft tissue of the sample as proposed in [8].

MATERIALS AND METHODS

A. Forward model

We model the measurements as independently distributed Poisson random variables [13] contaminated by extra background counts, primarily scatter:

$$Y_i \sim \text{Poisson} \{ \bar{Y}_i \}, i = 1, \dots, N \quad (1)$$

with

$$\bar{Y}_i = \int I_i(\varepsilon) e^{-\int_{L_i} \mu(\varepsilon) dl} d\varepsilon + r_i \quad (2)$$

where $\mu(\varepsilon)$ is the attenuation coefficient at each energy ε , the integral in the exponent is taken over the line L_i

Manuscript received April 2, 2018. This work was partially supported by the Ministry of Economy, Industry and Competitiveness (DPI2016-79075-R) and ISCIII-FIS grants DTS17/00122, co-financed by ERDF (FEDER) Funds from the European Commission, “A way of making Europe”. The CNIC is supported by the Ministry of Economy, Industry and Competitiveness (MEIC) and the Pro CNIC Foundation, and is a Severo Ochoa Center of Excellence (SEV-2015-0505).

C. Martinez, M. Abella and M. Desco are with the Dpto. Bioingeniería e Ingeniería Aeroespacial, Universidad Carlos III de Madrid and the Instituto de Investigación Sanitaria Gregorio Marañón, Madrid, España (e-mail: mabella@ing.uc3m.es, cmartinez@hggm.es).

J. A. Fessler is with Electrical Engineering and Computer Science department, The University of Michigan, Ann Arbor, MI 48109-2122, USA.

M. Abella and M. Desco are with the Centro Nacional de Investigaciones Cardiovasculares Carlos III (CNIC), Madrid, España (e-mail: manuel.desco@cnic.es).

M. Desco is with the Centro de investigación en red salud mental (CIBERSAM), Madrid, España. (e-mail: desco@hggm.es).

followed by the ray, and $I_i(\varepsilon)$ is the incident intensity and the term r_i accounts for mean scatter and mean other background signals for the i -th ray.

Following [4, 14] we model the attenuation coefficient in Eq. 2 at each pixel j as:

$$\mu_j(\varepsilon) = \sum_{k=1}^K \text{mac}_k(\varepsilon) f_k^j \rho_j \quad (3)$$

where mac_k is the mass attenuation coefficient of the material k , ρ the density and f_k^j is a unitless fraction that describes the contribution of the material k to attenuation in the pixel j . We assume $K=2$, i.e., the object contains only soft tissue (ST) and bone (B). The contribution of each tissue type to the line integral along the i -th ray is:

$$t_{ST}(\rho) = \sum_{j=1}^p a_{ij} f_{ST}^j(\rho_j) \rho_j \quad (4)$$

$$t_B(\rho) = \sum_{j=1}^p a_{ij} f_B^j(\rho_j) \rho_j \quad (5)$$

where a_{ij} are the elements of the system matrix. Here we allow the unitless fraction (f_k^j) to only be 1 or 0, i.e., the pixels do not contain mixtures of tissues. Eq. 2 for the expected value of the measured data along the path i results in:

$$\begin{aligned} \bar{Y}_i(\rho) &= \int I_i(\varepsilon) e^{-\int_{L_i} \mu(\varepsilon) dl} d\varepsilon + r_i = \\ &= I_i e^{-F(t_{ST}^i(\rho), t_B^i(\rho))} + r_i \end{aligned} \quad (6)$$

where

$$I_i \equiv \int I_i(\varepsilon) d\varepsilon \quad (7)$$

and the beam-hardening function, F , is:

$$F(t_{ST}, t_B) = -\log \int \frac{I(\varepsilon)}{I} e^{-\text{mac}_{ST}(\varepsilon)t_{ST} - \text{mac}_B(\varepsilon)t_B} d\varepsilon \quad (8)$$

dropping the dependence on ray i for simplicity.

B. Beam-Hardening function

The beam-hardening function $F(t_{ST}, t_B)$ could be analytically calculated from a known spectrum, but often this information is not available. To avoid assuming spectrum knowledge, the proposed method determines $F(t_{ST}, t_B)$ experimentally using the acquired data following the process outlined in Fig. 1.

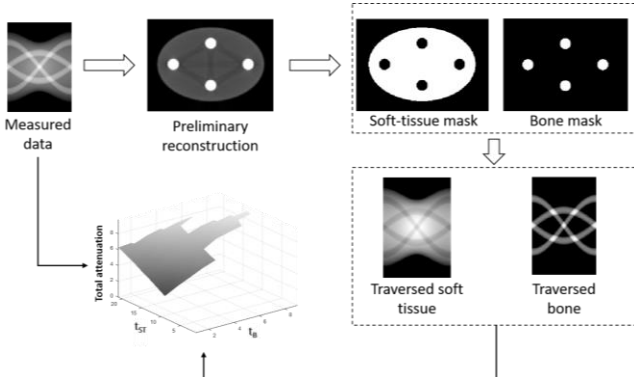


Fig. 1. Workflow for the generation of the beam-hardening function.

First bone and soft-tissue masks are obtained by thresholding a preliminary reconstructed image. These two masks are then multiplied by the density of each tissue and projected, which will be the x and y axis, where x corresponds to t_{ST} and y corresponds to t_B . The value in the original projection will be the z axis, corresponding to $F(t_{ST}, t_B)$.

The generated $F(t_{ST}, t_B)$ will not cover the whole space, since a specific acquisition will not have all possible combinations of soft tissue and bone (Fig. 2, left). To completely characterize the beam-hardening function, we “extrapolate” the incomplete function F using a quadratic function (Fig. 2, right).

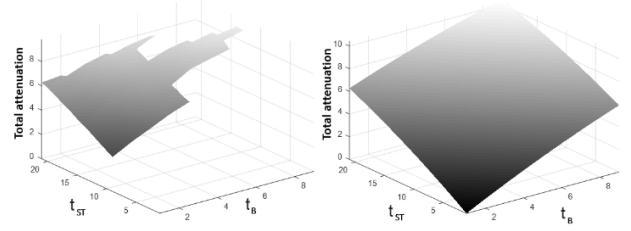


Fig. 2. Measured (left) and extrapolated (right) beam-hardening function.

C. Cost function

The negative log-likelihood for independent Poisson measurement is:

$$L(\rho) = -\sum_{i=1}^N h_i \left(F(t_{ST}(\rho), t_B(\rho)) \right) \quad (9)$$

where

$$h_i(d) = -Y_i \log(I_i e^{-d} + r_i) + I_i e^{-d} + r_i \quad (10)$$

Since minimizing $L(\rho)$ is generally an ill-posed problem, regularization is included by adding a penalty term to control how much the object ρ departs from our assumptions about image properties. In this work, we use a 3D roughness penalty function with the convex edge-preserving Huber potential. The resulting penalized cost function is:

$$\Phi(\rho) = L(\rho) + \beta R(\rho) \quad (11)$$

where β is a scalar that controls the tradeoff between the data-fit and penalty terms.

D. Algorithm

We derive an iterative algorithm based on separable quadratic surrogates using the principles of optimization transfer [14], resulting in the following update:

$$\rho^{n+1} = \rho^n - D^{-1} \nabla \Phi(\rho^n) \quad (12)$$

where D is a diagonal matrix that influences the rate of convergence. We originally designed D to ensure that the algorithm monotonically decreases the cost function. As in [9], in practice we choose the elements of D approximately by using the precomputed curvature:

$$d_j = \left(\text{mac}_{ST}^2(\varepsilon_{eff}) + \text{mac}_B^2(\varepsilon_{eff}) \right) \sum_{i=1}^N a_{ij} \sum_j a_{ij} Y_i \quad (13)$$

where the effective $mac(\varepsilon_{eff})$ values for each tissue are approximated using the derivative of beam-hardening function at $(0,0)$.

Artifacts in the preliminary reconstruction may hinder the segmentation to obtain the bone and soft-tissue masks, resulting in an erroneous beam-hardening function. To tackle this problem, new bone and soft-tissue masks are obtained from the solution at each iteration and are used to recalculate the beam-hardening function.

EVALUATION

Preliminary evaluation used simulations of a 2D phantom with two cortical bone inserts having density 1.9 gr/cm^3 , one trabecular bone insert with density 1.5 gr/cm^3 and one adipose-tissue insert with density 0.9 gr/cm^3 , inside of a soft-tissue ellipse with density 1.06 gr/cm^3 (Fig. 3).

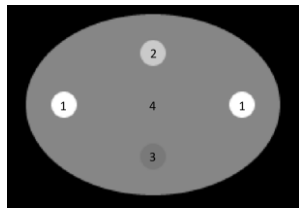


Fig. 3. Test phantom with two cortical bone inserts (1), one trabecular bone insert (2), and one adipose-tissue insert (3) inside of a soft-tissue ellipse (4).

Four polyenergetic X-ray datasets were generated using MIRT (<http://www.eecs.umich.edu/~fessler/code/index.html>) with a 50 kVp spectrum and 0.1 mm aluminum filtration, typically used in preclinical studies. The number of counts per ray were 10^5 and 10^6 to simulate low-SNR and high-SNR scenarios respectively. For each scenario, we obtained 45 and 180 projections in a span of 180 degrees with a matrix size of 256×256 pixels and 0.1×0.1 mm pixel size.

The data were reconstructed with FBP, with FBP corrected by the free calibration method (fCM) proposed in [8] and by the proposed statistical algorithm.

RESULTS

Fig. 4 shows the segmented soft-tissue mask along different iterations for the low-SNR scenario with 45 projections. The mask in the first iteration has holes due to the streaks from beam-hardening effect and low sampling, which are removed in subsequent iterations.



Fig. 4. Soft tissue mask in iteration 1 (left), 5 (center) and 15 (right).

Fig. 5 shows the results for 180 projections. The result of FBP corrected with fCM shows a good compensation of beam-hardening artifacts but it fails to correct streaks with high noise (low SNR scenario), while the proposed method results in good quality reconstructions in high-SNR and low-SNR scenarios.

When the number of projection is reduced to 45 (Fig. 6) FBP+fCM eliminates the beam hardening artifacts in the high-SNR scenario, but the reconstruction is contaminated with streaks due to the lack of projections. For the low-SNR scenario, FBP+fCM also fails to compensate the streaks due to beam-hardening effect, because of the wrong segmentation used to create the beam-hardening function. The proposed method eliminates the beam hardening and the streaks in all cases.

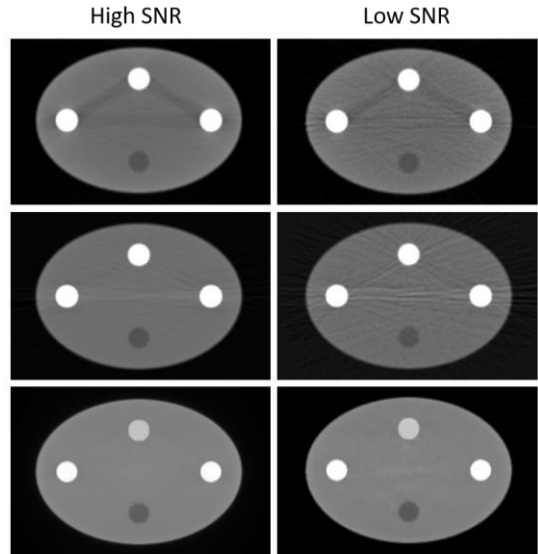


Fig. 5. Results for the 180 projections datasets using FBP (top), FBP + fCM (center) and the proposed algorithm (bottom).

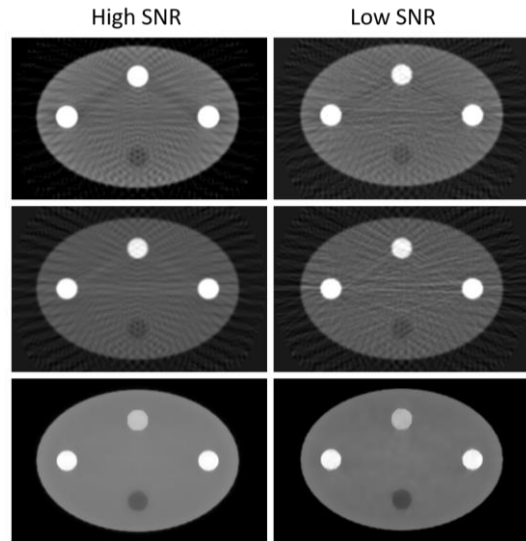


Fig. 6. Results for the 45 projections datasets using FBP (top), FBP +fCM (center) and the proposed algorithm (bottom).

CONCLUSIONS

We present a new statistical reconstruction algorithm that includes beam-hardening correction without needing any spectrum knowledge or correction parameters optimization.

The method models the polychromatic effect via a beam-hardening function determined from the acquired data and a segmentation of bone and soft-tissue masks, which are

iteratively improved. Results on simulated data show a reduction of streaks due to both beam-hardening effect and low number of projections.

REFERENCES

- [1] J. F. Barrett and N. Keat, "Artifacts in CT: Recognition and Avoidance," *RadioGraphics*, vol. 24, pp. 1679-1691, 2004.
- [2] R. A. Brooks and G. D. Chiro, "Beam hardening in x-ray reconstruction tomography," *Phys. Med. Biol.*, vol. 21, pp. 390-8, 1976.
- [3] O. Nalcioglu and R. Y. Lou, "Post-reconstruction Method for Beam Hardening in Computerised Tomography," *Phys. Med. Biol.*, vol. 24, pp. 330-40, 1979.
- [4] P. M. Joseph and R. D. Spital, "A method for correcting bone induced artifacts in computed tomography scanners," *J. Comp. Assisted Tomo.*, vol. 2, pp. 100-8, 1978.
- [5] Y. Kyriakou, E. Meyer, D. Prell, and M. Kachelrieß, "Empirical beam hardening correction (EBHC) for CT," *Med Phys*, vol. 37, pp. 5179-5187, 2010.
- [6] S. Schüller, S. Sawall, K. Stannigel, M. Hülsbusch, J. Ulrici, E. Hell, *et al.*, "Segmentation-free empirical beam hardening correction for CT," *Med Phys*, vol. 42, pp. 794-803, 2015.
- [7] C. Martinez, C. De Molina, M. Desco, and M. Abella, "Simple method for beam-hardening correction based on a 2D linearization function," in *The 4th International Meeting on Image Formation in X-Ray Computed Tomography (CTMeeting 2016)*, Bamberg, Germany, 2016.
- [8] C. Martínez, C. de Molina, M. Desco, and M. Abella, "Calibration-free method for beam-hardening compensation: preliminary results," in *Nuclear Science Symposium and Medical Imaging Conference (NSS/MIC)*, Atlanta, GA, 2017.
- [9] I. A. Elbakri and J. A. Fessler, "Statistical Image Reconstruction for Polyenergetic X-Ray Computed Tomography," *IEEE Trans. Med. Imaging*, vol. 21, pp. 89-99, 2002.
- [10] I. A. Elbakri and J. A. Fessler, "Segmentation-free statistical image reconstruction for polyenergetic x-ray computed tomography with experimental validation," *Phys. Med. Biol.*, vol. 48, pp. 2453-77, 2003.
- [11] S. Srivastava and J. A. Fessler, "Simplified statistical image reconstruction algorithm for polyenergetic X-ray CT," presented at the IEEE Nuclear Science Symposium Conference Record, 2005.
- [12] M. Abella and J. A. Fessler, "A new statistical image reconstruction algorithm for polyenergetic X-ray CT," *Proceedings of the 2009 IEEE International Symposium on Biomedical Imaging (ISBI)*, pp. 165-8, 2009.
- [13] H. Erdogan and J. A. Fessler, "Monotonic algorithms for transmission tomography," *IEEE Trans. Med. Imaging*, vol. 18, pp. 801-14, 1999.
- [14] R. E. Alvarez and A. Macovski, "Energy-selective reconstruction in x-ray computerized tomography," *Phys. Med. Biol.*, vol. 21, pp. 733-44, 1976.